A Biophysical Model of Visual Rivalry Links Cellular Mechanisms to Signatures of Conscious Perception

Christopher J. Whyte[1,2], Brandon R. Munn[1,2], Jaan Aru[3], Matthew Larkum[4,5], Yohan John[6], Eli J. Müller[1,2], and James M. Shine[1,2]

Affiliations

[1]Brain and Mind Center, The University of Sydney, Sydney, Australia.

[2]Complex Systems, School of Physics, The University of Sydney, Sydney, Australia.

[3]Computational Neuroscience Lab, University of Tartu, Tartu, Estonia.

[4]Institute for Biology, Humboldt University of Berlin, Berlin, Germany.

[5]NeuroCure Cluster of Excellence, Charité – Universitätsmedizin Berlin, Berlin, Germany.

[6]Neural Systems Laboratory, Department of Health Sciences, Boston University, Boston, MA, USA.

Corresponding author address

James M. Shine

Brain and Mind Centre

94 Mallett St, Camperdown, NSW, 2050

Email: mac.shine@sydney.edu.au

Abstract

Investigations into the neural basis of conscious perception span multiple scales and levels of analysis. There is, however, a theoretical and methodological gap between advances made at the microscopic scale in animal models and those made at the macroscopic scale in human cognitive neuroscience that places a fundamental limit on our understanding of the neurobiological basis of consciousness. Here, we use computational modelling to bridge this gap. Specifically, we show that the same mechanism that underlies threshold detection in mice – apical dendrite mediated burst firing in thick-tufted layer V pyramidal neurons – determines perceptual dominance in a thalamocortical model of binocular rivalry – a staple task in the cognitive neuroscience of consciousness. The model conforms to the constraints imposed by decades of previous research into binocular rivalry and generalises to the more sophisticated rivalry tasks studied in humans generating novel, testable, explanations of the role of expectation and attention in rivalry. Our model, therefore, provides an empirically-tractable bridge between cellular-level mechanisms and conscious perception.

Introduction

Uncovering the neural mechanisms of conscious perception and conscious state remains one of the great outstanding challenges in modern neuroscience. In spite of the rich backdrop of existing theoretical and experimental work (e.g., Brown et al., 2019; Lamme, 2006; Mashour et al., 2020; Tononi et al., 2016), there is limited interaction between theories proposed at different scales (Seth & Bayne, 2022). Perhaps most tellingly, it is rare for empirical predictions at one scale to be brought into contact with predictions at other scales: the large-scale correlates of consciousness are rarely couched in terms of their putative cellular underpinnings (and *vice versa*). This is not without good reason. Cognitive neuroscience is largely based on human neuroimaging, where high-resolution (i.e., layer specific) recordings and precise causal manipulations (e.g., optogenetic and pharmacological) are exceedingly difficult and often impossible. In turn, although it is possible to obtain high-resolution data with precise causal control in animal models they are enormously restricted in the range and complexity of tasks that they can perform. For instance measures of perception rely on indirect behavioural read-outs, limiting contact with predictions associated with the richer and more nuanced features of our conscious experience.

Here we use biophysical modelling to bridge the gap between the thalamocortical circuit identified in a recent rodent model of perception (Aru, Suzuki, et al., 2020; Takahashi et al., 2016, 2020) and the behavioural signatures of conscious perception studied in cognitive neuroscience. Specifically, we built a spiking neural network model of binocular rivalry based on a circuit comprising thick-tufted LV pyramidal tract (LV_{PT}) neurons whose burst-firing state is gated by non-specific matrix thalamus, and is known to play a causal role in both perception and conscious state (Aru et al., 2019; Aru, Siclari, et al., 2020; Aru, Suzuki, et al., 2020; Takahashi et al., 2016, 2020). We chose binocular rivalry as the primary explanatory target of the model as it is a staple task in the cognitive neuroscience of consciousness (Overgaard, 2015) that has been studied extensively in both empirical (Alais & Blake, 2005; Blake & Tong, 2008; Carmel et al., 2010; Tong et al., 2006) and computational (Grossberg et al., 2008; Laing et al., 2010; Laing & Chow, 2002; Safavi & Dayan, 2022; Shpiro et al., 2007, 2009; Wilson, 2003, 2007, 2017) settings, thereby imposing a wealth of constraints on the modelling process. In addition, due to recent advances in experimental paradigms aspects of visual rivalry can now

be studied in mice (Bogatova et al., 2022; Palagina et al., 2017), making it possible to propose testable predictions at both microscopic and macroscopic scales.

Our novel neurobiological approach to modelling allowed us: i) to explore whether cellular-level mechanisms could recover the lawlike psychophysical relationships between stimulus properties and perceptual phenomenology known to characterise binocular rivalry (Brascamp et al., 2015); ii) to interrogate the putative cellular basis of perceptual dominance through a series of in silico perturbation experiments; and finally, iii) to test the generalisability of the cellular mechanisms to the more sophisticated visual rivalry tasks studied in humans which manipulate cognitive constructs such as attention (Paffen & Alais, 2011) and expectation (Pinto et al., 2015). In this way, our model provides a biophysical bridge between cellular-level mechanisms and the behavioural signatures of consciousness studied in human cognitive neuroscience.

Results

The dynamical elements of the model consisted of three classes of neurons – LV_{PT} cells, fast spiking interneurons (basket cells), and matrix thalamus cells (**Fig 1 A-B)** – each of which were modelled using biophysically plausible spiking neurons (Izhikevich, 2003, 2004, 2006). The parameters of the basket cells and thalamus cells were taken unmodified from the whole brain model of Izhikevich and Edelman (2008). To capture the unique context-dependent bursting behaviour of the LV_{PT} cell (Larkum, 2004, 2022; Larkum et al., 2009), we created a novel dual-compartment variation of the Izhikevich neuron with (coupled) apical and somatic compartments. This allowed us to reproduce the behaviour of these cells that has been linked to conscious perception – namely, the change in dynamical regime in LV_{PT} cells that occurs when these cells receive coincident into their apical and basal dendrites. Specifically, we leveraged the insight (Izhikevich, 2003; Munn et al., 2023) that the difference between regular spiking and bursting behaviour (operationally defined by shorter inter spike intervals) can be modelled by changing the reset conditions of the somatic compartment – raising the reset voltage taking the neuron closer to threshold and reducing the magnitude of spike adaptation. We arranged the coupling between compartments such that the apical compartment controlled the reset conditions on the somatic compartment, with an apical spike causing a switch in the

reset conditions of the somatic compartment from regular spiking to bursting parameters for 25 ms (in line with empirical measurements; Larkum, 2004). The membrane potential of the apical compartment was coupled to the somatic compartment through a conductance term allowing for somatic spikes to back propagate and contribute to the generation of apical spikes. In line with empirical findings and previous modelling (Larkum, 2004; Shai et al., 2015), the spiking activity in the apical compartment effectively controlled the gain of the somatic compartment's FR curve through increasing the amount of time each LV_{PT} cell spent in the bursting regime rather than the regular spiking regime (**Fig 1C**).

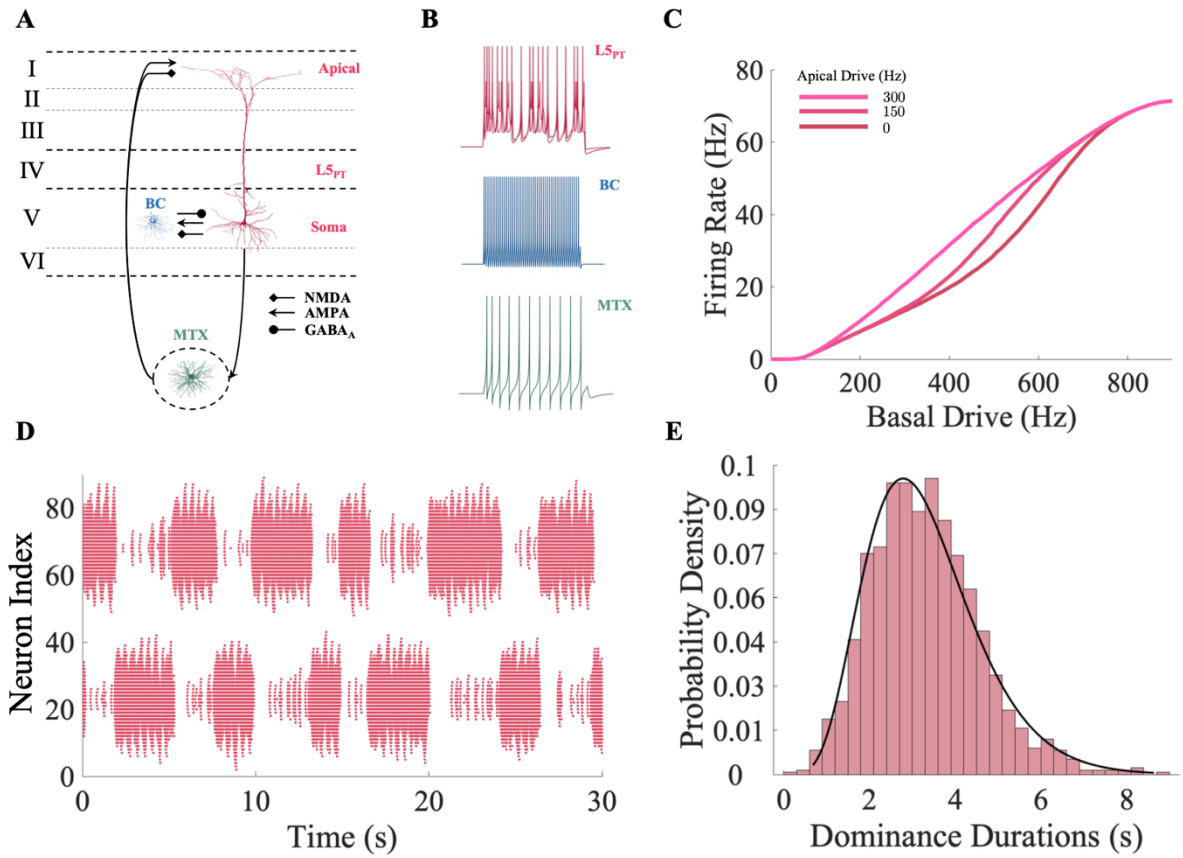

Figure 1. A) Anatomy of the model thalamocortical loop connecting non-specific matrix thalamus and LV_{PT} neurons. **B)** Single neuron dynamics of each class of cell used in the model. **C)** Firing rate of the novel dual compartment LV_{PT} neuron as a function of basal drive and apical drive. **D)** Example raster plot of the stochastic oscillations in somatic firing rate in the LV_{PT} neuron as the model is shown orthogonal grating stimuli. **E)** Example histogram of dominance durations for a simulation run with 475 Hz of basal drive. Black line shows the fit of a Gamma distribution with parameters estimated via MLE ($\alpha = 6.3546$, and $\beta = 2.1209$, where the Gamma distribution is given by $f(x) = \beta^{\alpha}\Gamma(\alpha)^{-1}x^{\alpha-1}e^{-\beta x}$). Across basal drive conditions, comparison of negative log likelihoods showed that the distribution of dominance durations was best fit by a Gamma distribution ($\ell = 9.7562 \times 10^{-4}$), compared to lognormal ($\ell = 9.9370 \times 10^{-4}$), or normal distributions ($\ell = 1.0053 \times 10^{-5}$).

Based on previous spiking neural network models of rivalry (Laing et al., 2010; Laing & Chow, 2002; Wang et al., 2020), we used a one-dimensional ring architecture (90 pairs of LV_{PT} excitatory and fast-spiking inhibitory interneurons) to wire together the cortical components of the network. Each point on the ring represents an orientation preference, with one full rotation around the ring corresponding to a 180° visual rotation. This provided each neuron with a 2° difference in orientation preference, relative its neighbours. The (dimensionless) synaptic weights connecting neurons on the ring had a spatial Gaussian connectivity with synaptic weight decaying as a function of the Euclidean distance between neurons. The synapses themselves had a bi-exponential form, with rise and decay time parameters chosen to recapitulate the dynamics of inhibitory ($GABA_A$), and excitatory (AMPA and NMDA) conductance (Dayan & Abbott, 2005; Gerstner et al., 2014). For a full description see online methods.

Throughout this paper we draw on data from a wide array of experiments. Despite it being possible to fit the parameters of our model to each experimental finding individually this approach permits of too many degrees of freedom and risks over interpreting idiosyncratic aspects of individual experiments. Instead, in the spirit of hypothesis driven science, we elected to explore if a single model could qualitatively reproduce a wide array of experimental findings with a minimal set of parameter changes carefully chosen to reflect experimental manipulations and perturbations. We began by simulating a standard rivalry experiment, driving the model with input representing orthogonal gratings presented to each eye. External drive into the model exclusively targeted the basal dendrites of the somatic compartment of LV_{PT} cells and was weighted by a spatial Gaussian centred on neurons 90° apart on the ring (i.e., 45 neurons apart) mimicking the orthogonal grating stimuli commonly employed in binocular rivalry experiments (e.g., Logothetis & Leopold, 1996; Tong et al., 2006). In line with previous modelling work, we interpreted persistent 'bumps' of activity on the ring as representing 'perception'. In agreement with previous models and psychophysical data (Wilson, 2003; Wolfe, 1983), at stimulus onset there was a brief period lasting ~150 ms where neuronal populations on both side of the ring were equally dominant before the competition between populations for dominance was resolved and the model settled into an oscillatory regime where one of the two populations was dominant whilst the other was suppressed (**Fig 1D**). Also in agreement with psychophysical data, switches between persistent activity and suppression

(perceptual reversals) appeared stochastic, with a right-skewed distribution of dominance durations that was well described by a gamma distribution (Brascamp et al., 2015; Levelt, 1967; Logothetis & Leopold, 1996; **figure 1E**). We found that the dynamical regime underlying these stochastic oscillations consisted of noisy excursions around a stable limit cycle (**supplementary material Fig S1)**.

Levelt's Propositions

We next sought to validate the model by reproducing Levelt's propositions (Brascamp et al., 2015) – a set of four statements that compactly summarise the lawlike relationship between stimulus strength (e.g., luminance contrast, colour contrast, stimulus motion) and the phenomenology of binocular rivalry. Here, we focus on the second and fourth propositions, as they constitute the "core laws" of rivalry (propositions one and three are direct consequences of proposition two; Brascamp et al., 2015). Levelt's second proposition states that increasing the difference in stimulus strength between the two eyes will principally increase the average dominance duration of the percept associated with stronger stimulus (Brascamp et al., 2015), a finding that has been shown to hold across studies in both human and non-human primates (e.g., Leopold & Logothetis, 1996; Logothetis & Leopold, 1996). According to Levelt's fourth proposition, increasing the strength of the stimulus delivered to both eyes will increase the average perceptual reversal rate (i.e., decrease dominance durations; Brascamp et al., 2015), a finding that, like Levelt's second proposition, has been replicated across a wide array of experimental settings (Bonneh et al., 2014; Brascamp et al., 2006; Buckthought et al., 2008; Meng & Tong, 2004). Originally proposed in 1965 (Levelt, 1965), these psychophysical "laws" have proven to be remarkably robust needing only minor modification and contextualisation (Brascamp et al., 2015). Levelt's propositions have historically therefore served as a benchmark for computational models of rivalry (e.g., (Grossberg et al., 2008; Laing & Chow, 2002; Shpiro et al., 2007; Wilson, 2007).

To simulate the experimental conditions described by Levelt's second proposition, we presented the model with external drive centred on neurons with orthogonal orientation preferences and then decreased the spike rate entering one side of the ring in steps of 20 Hz across simulations. In line with Levelt's second proposition (**Fig 2A**), the average dominance

duration of the percept corresponding to the stronger stimulus showed a steep increase from ~2.75 s with matched input, to ~4.5 s with maximally different input whilst the average dominance duration on the side of the weakened stimulus decreased comparatively gradually to ~2.1 s with maximally different inputs.

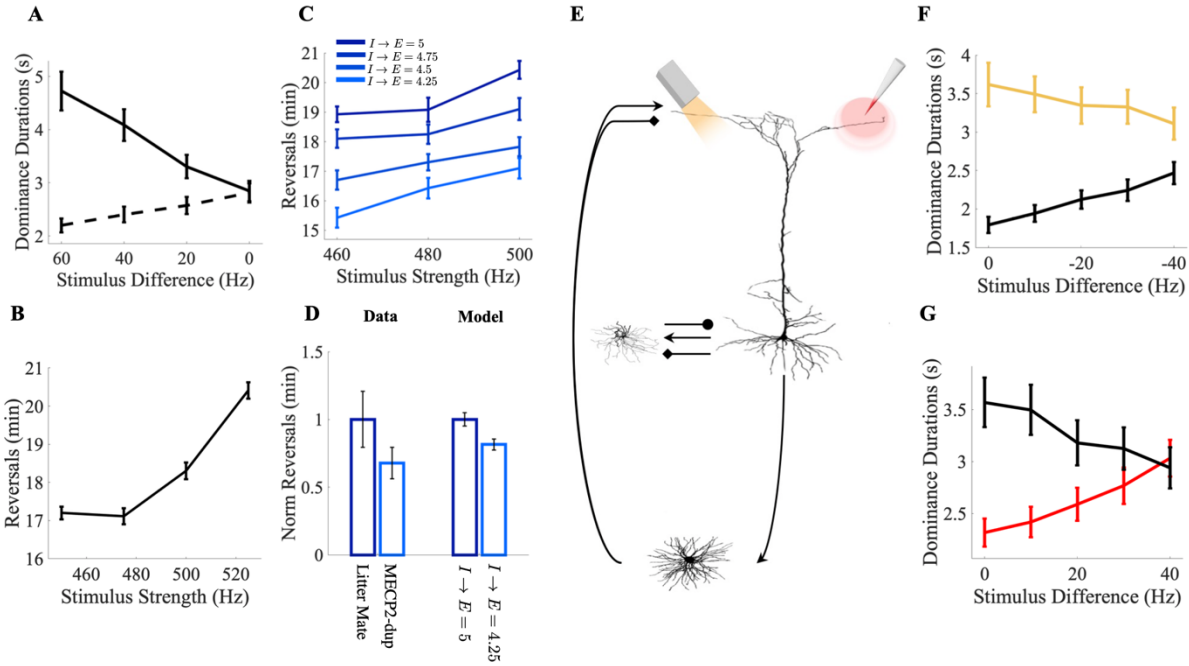

Figure 2. A) Simulation of Levelt's second proposition. Solid line shows dominance duration of the population receiving the fixed external drive (520 Hz). Dash line shows the dominance duration of the population receiving the decreasing external drive. **B)** Simulation of Levelt's fourth proposition. Perceptual reversals (per minute of simulation time) increase as a function of external drive. **C)** Effect of EI balance on perceptual reversal frequency across external drive frequencies. Increasing the magnitude of $I \to E$ coupling speeds rivalry. **D)** Comparison of empirical data acquired from figure 1 of Bogatova et al, (2022) comparing reversal frequency between mice with and without a MECP2-duplication (which predominantly effects GABAergic signalling; Chao et al., 2010) with model output for $I \to E = 4.25$ and $I \to E = 5$. Reversal frequency was normalised by the max value of the mean. **E)** Model thalamocortical loop highlighting the perturbation to apical dendrites designed to mimic optogenetic excitation (yellow), and puff application of baclofen (red). **F)** Dominance duration as a function of the difference in external drive entering the excited population. Yellow line shows the dominance duration of the population with excited apical dendrites and decreasing basal drive. Black line shows the dominance duration of the population with unperturbed apical dendrites and fixed basal drive. **G)** Dominance duration as a function of the difference in external drive entering the inhibited population. Red line shows the dominance duration of the population with inhibited apical dendrites and increasing basal drive. Black line again shows the dominance duration of the population with unperturbed apical dendrites and fixed basal drive. In all plots error bars show the standard error of the mean.

To simulate Levelt's fourth proposition we ran a series of simulations in which we increased the spike rate of the external drive in steps of 25 Hz across simulations. In line with Levelt's propositions (**Fig 2B**), the perceptual reversal rate increased with input strength, starting at ~17 reversals per minute at the weakest stimulus and increasing to ~20.5 for the strongest. We thus confirmed that our neurobiologically detailed model of the thalamocortical loop is capable of reproducing Levelt's propositions, which together with the Gamma distribution of dominance durations, show the consistency of our model with the key lawlike psychophysical relationships known to characterise binocular rivalry.

In Silico Cellular Perturbations

Having confirmed that our model conforms to psychophysical constraints, we next sought to interrogate the cellular mechanisms of perceptual dominance through a series of *in silico* perturbation experiments designed to: i) test the consistency of our model with genetic perturbations of EI balance studied in a mouse model of visual rivalry by Bogatova et al, (2022); and ii) interrogate the novel burst-dependent mechanism of perceptual dominance by mimicking the optogenetic and pharmacological experiments carried out by Takahashi et al, (2016, 2020) in the context of threshold detection that originally motivated the hypothesis that the bursting of LV_{PT} cells is the mechanism of conscious perception (Aru et al., 2019; Aru, Suzuki, et al., 2020).

Leveraging a mouse model of visual rivalry Bogatova et al, (2022) found that compared to non-transgenic litter mates, mice with a MECP2-duplication (that predominantly affects GABAergic signalling; Chao et al., 2010) showed a reduced rate of perceptual reversals (**Fig 2D**) which they hypothesise as being caused by a reduction in the relative strength of cortical inhibition. To test this in our model we ran a series of simulations across a range of $I \rightarrow E$ magnitudes, and external drive frequencies. Consistent with the empirical data, and in support of the reduced inhibition hypothesis, across a range of external drive conditions reducing the magnitude of inhibitory signalling reduced the rate of perceptual reversals (**Fig 2 C-D**).

Next, we turned to the role of apical spikes on dominance durations. Based on the gain modulating effect of apical spikes (**Fig 1C**), we hypothesised that exciting/inhibiting the apical

dendrites should be approximately equivalent to increasing/decreasing basal drive. Specifically, we predicted that artificially exciting the apical dendrites of a population should be comparable to an increase in basal drive to that population (and *vice versa* for inhibition). This led to the novel prediction that exciting the apical dendrites on one side of the ring should lead to an increase in dominance durations for the corresponding percept, and importantly, that we should be able to compensate for this increase by decreasing the basal drive into that population a relationship that should also hold in reverse for inhibition of apical dendrites. To test this hypothesis in our model, we added a constant source of external drive ($\pm$ 100 pS) to the apical dendrites on one side of the ring that was designed to mimic optogenetic excitation or pharmacological inhibition (e.g., via puff application of baclofen) of the apical dendrites within an ocular dominance column (**Fig 2E**). In agreement with our hypothesis, excitation of the apical dendrites led to a substantial jump in the average dominance duration of the excited population, which gradually decreased (i.e., could be compensated for) by decreasing basal drive into excited side of the ring (**Fig 2F**). Similarly, inhibition of the apical dendrites led to a dramatic increase in the dominance durations of the uninhibited population that gradually decreased as basal input into the inhibited side of the ring was increased (**Fig 2G**).

These *in silico* perturbation experiments serve a dual purpose. First, they catalyse the link between theory and empirical investigation by reproducing existing data on the role of EI balance in mouse models of visual rivalry, and provide a strong empirical prediction that can be tested in a mouse model. Second, they highlight the importance of dendrite-mediated bursting in the determination of perceptual dominance. In this way, our results suggest a potential explanation for cognitive constructs, such as attention and expectation, both of which have both been shown to modulate dominance durations (Denison et al., 2011; C. Paffen & Alais, 2011; Pinto et al., 2015), and have independently been connected to key neuroanatomical components of the model (e.g., non-specific matrix thalamus in the case of attention and cortical feedback in the case of expectation; (Friston, 2018; Halassa & Kastner, 2017; Kastner et al., 2020).

Attention and Expectation as Apical Gain Control

Building on the insights gained through our *in silico* perturbation of the model in a basic binocular rivalry task, we next sought to interrogate the generality of the mechanism of apical burst control in the context of the more sophisticated tasks used in human cognitive neuroscience to study the role of attention and expectation in visual rivalry.

The non-specific matrix thalamus has been linked to attention (Halassa & Kastner, 2017; Shine et al., 2023), specifically through the selective boosting of cortical responses to feed forward input through the formation of a recurrent loop with LV_{PT} cells (Guo et al., 2020; Mease & Gonzalez, 2021; Wimmer et al., 2010; **Fig 3A**). Indeed, in non-human primates, inhibition of the pulvinar (a region containing a high proportion of matrix cells) diminishes cortical responses to task relevant stimuli (Zhou et al., 2016), lesions to pulvinar result in an inability to ignore distractors (Kastner et al., 2020), and in rodents increasing the excitability of medial dorsal nuclei (again a region containing matrix-like cells) increases cortical excitability (Schmitt et al., 2017). In the context of binocular rivalry, attention modulates the relationship between dominance durations and stimulus strength. Specifically, reminiscent of Levelt's second proposition, by attending to one stimulus it is possible to selectively increase the average dominance duration of the attended percept (Meng & Tong, 2004; Paffen & Alais, 2011). Similarly, analogous to Levelt's fourth proposition, in a series of two experiments Paffen et al, (2006) showed that when attention was removed from both rivalry stimuli, through the addition of a motion discrimination distractor task (**Fig 3B**), the rate of perceptual reversals was slowed as a function of the difficulty of the distractor task. They then repeated the task across a range of stimulus contrasts and found that attending to the rivalry stimulus through the removal of the distractor task was equivalent to an increase in stimulus contrast with the authors positing a gain control mechanism of attention as an explanation (also see John et al., 2018; Paffen & Alais, 2011).

Based upon these behavioural results and the aforementioned anatomical considerations, we hypothesised that the role of attention in rivalry could be reproduced in our model by selectively modulating the magnitude of thalamic feedback onto apical dendrites, which, consistent with the gain control mechanism posited by Paffen et al, (2006), should speed perceptual reversals equivalently to an increase in external drive. To test this hypothesis, we conducted a series of simulations in which we increased the spike rate of the external drive and

the magnitude of thalamic feedback stepwise across simulation. In line with our hypothesis, at a fixed external drive, stepwise increases in the magnitude of thalamic feedback resulted in a stepwise increase the rate of perceptual reversals recapitulating the parametric effect of distractor task difficulty (**Fig 3C**). Similarly, across the full range of external drive rates, we found that increasing the magnitude of thalamic feedback from 5 to 8 was approximately equivalent to a 15 Hz increase in external drive (**Fig 3 D-E**).

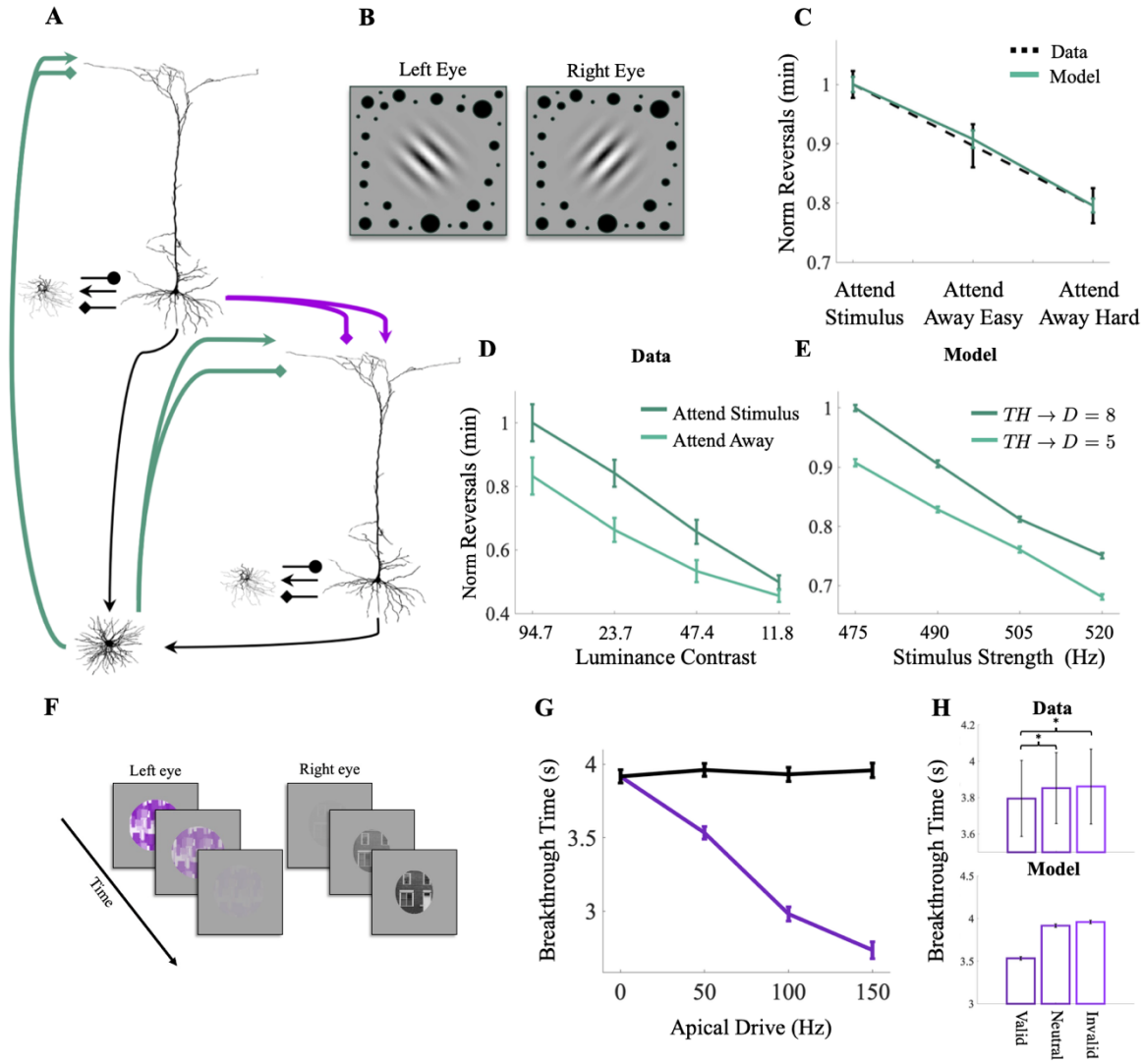

Figure 3. A) Model thalamocortical loop highlighting the closed loop projections from non-specific matrix thalamus to the apical dendrites of LV_{PT} neurons (green) and the projections from deep layers of "higher" regions of the cortical hierarchy to superficial layers of "lower" cortical regions (purple) represented in our simulations by an (additional) external source of apical drive. **B)** Modified binocular rivalry task of Paffen et al, (2006). Motion discrimination distractor task in periphery required participants to track the overall direction of the moving dots allowing them to remove attention in a parametric manner. **C)** Comparison of empirical data taken from figure 1A of Paffen et al, (2006) and model output. The allocation of attention to the rivalry stimuli was modelled through a stepwise increase in the magnitude of thalamic feedback to the apical dendrites $\lambda^{TH \rightarrow D} = 1, 5, 8$.

Reversal frequency was normalised by the max value of the mean. **D)** Empirical data of Paffen et al, (2006) adapted from figure 1C showing the equivalence between the allocation of attention and a stepwise increase in stimulus contrast. **E)** Model output of simulation designed to mimic the experiment of Paffen et al, (2006). **F)** Continuous flash suppression task of Pinto et al, (2015), mask stimulus entering one eye starts at full contrast and linearly decreases whilst the house stimulus entering the other eye starts at zero contrast and gradually increases. All trials start with a cue (not shown) which probabilistically indicats the category (e.g. face or house) of the low contrast stimulus. Pinto et al, (2015) used a range of response conditions including detection, identification, recognition, and breakthrough. As our model does not have the granularity to distinguish between these types of decision criteria we focus on experiment 4 which examined breakthrough time. **G)** Model breakthrough times as a function of apical drive (Hz) for valid (purple) and invalid (black) expectation conditions. **H)** Comparison of empirical data of Pinto et al, (2015) experiment 4 (adapted from figure 5) with model breakthrough times. In all plots error bars show the standard error of the mean.

Expectation, like attention, has been linked to feedback projections terminating in superficial layers of cortex, however, in the case of expectation, the source of the feedback projections is hypothesized to originate from deep layers of anatomically "higher" cortical populations (Bastos et al., 2012, 2015, 2020; Friston, 2005, 2018; Grossberg, 1995; Raizada & Grossberg, 2003). In the context of rivalry, predictive cues shown before the onset of rivalry stimuli ultimately bias which stimulus wins the initial competition for dominance towards the expected stimulus (Denison et al., 2011; Valuch & Kulke, 2020). Similarly, in continuous flash suppression (**Fig 3F**) – a variation of visual rivalry where participants are presented with a high contrast image to one eye that gradually decreases in contrast and a low contrast image to the other eye that gradually increases in contrast – expectation has been shown to decrease the time it takes for the low contrast image to "break through" and dominate perception relative to invalid or no expectation (neutral) conditions, a finding that has been conceptually replicated across a range of experimental conditions (Pinto et al., 2015).

We hypothesised that the empirically observed effect of expectation could be reproduced by introducing an external source of apical drive to one side of the ring representing content specific predictive feedback elicited by a predictive cue. Specifically, breakthrough time should decrease as a function of apical drive by increasing the amount of time each neuron spends in burst mode and be unaffected by invalid expectations which target the apical dendrites of neurons receiving insufficient basal drive to emit a spike. To test this hypothesis, we introduced an additional source of external drive that targeted the apical compartment of the model.

To highlight the ability of our model to generalise beyond basic binocular rivalry paradigms, we focused our simulations on the continuous flash suppression finding. To model the effect of valid expectations, corresponding to a reliable predictive cue, we centred the Gaussian decay of the apical drive on the same orientation as either the left or right eye stimulus. Similarly, we modelled invalid expectations by centring the apical drive on an orientation half-way between the orientations of left and right eye stimuli targeting a portion of the ring that received almost no basal drive. In line with our hypothesis, breakthrough time decreased as a function of apical spike rate applied to orientation relevant locations, whereas invalid expectations (i.e. irrelevant orientation locations) had no effect on breakthrough time (**Fig 3G**). At low values of apical drive (50 Hz), breakthrough times for valid, neutral (i.e., no apical drive), and invalid expectations were comparable to empirical data (**Fig 3 H**). Together, these investigations confirm the validity of our model, and demonstrate how biophysical models can be used to connect cellular-level descriptions of conscious processing to cognitive constructs.

Discussion

The study of conscious perception in cognitive and cellular neuroscience has so far proceeded largely in parallel – the former exploring the largescale neural dynamics of conscious perception across a rich array of experimental settings, and the latter characterising the cellular circuitry of perception in exquisite detail, and with precise causal control, but in highly constrained experimental settings. Leveraging a neurobiologically detailed, model of the thalamocortical circuit, we have shown that a potential circuit-level mechanism of perceptual consciousness discovered in rodents (apical-mediation of bursting in LV_{PT} neurons; Aru et al., 2019, 2019; Takahashi et al., 2016, 2020) generalises to binocular rivalry a core task used to study conscious perception in cognitive neuroscience (Crick & Koch, 2003; Giles et al., 2016; Overgaard, 2015; Tong et al., 2006). In this way, we provide a roadmap for linking neuroscientific explanations of cognitive phenomena across spatial scales. A crucial aspect this process is striking the right balance between neurobiological detail and interpretability. In line with our goal of exploring the generality of apically-mediated bursting in LV_{PT} we only included the elements of the thalamocortical circuit directly implicated in empirical work linking LV_{PT} bursting to conscious perception.

The combination of neurobiological detail and transparency afforded by our model allowed us to simulate experimental interventions that would not be possible in human or non-human primates. In particular, we found that increasing the magnitude of $I \rightarrow E$ coupling reproduced the effect of genetic perturbations to EI balance on the frequency of perceptual reversals showing the consistency of out model with both human psychophysical data and data from cellular neuroscience. Further, in line with our apical gain control hypothesis, we found that simulated optogenetic excitation and pharmacological inhibition of apical dendrites produced similar imbalances in average dominance durations to those brought about by imbalances in basal drive. This suggested to us that changes in apical drive may underpin the effects of attention and expectation in visual rivalry both of which have both been shown to modulate dominance durations, and have independently been connected to non-specific matrix thalamus (Halassa & Kastner, 2017; Kastner et al., 2020; Schmitt et al., 2017; Shine et al., 2023; Zhou et al., 2016), and cortical feedback to superficial layers (Bastos et al., 2015, 2020; Friston, 2005, 2018), respectively. Indeed, we were able to reproduce the observed effect of attention (Paffen & Alais, 2011; Paffen et al., 2006) on rivalry by selectively modulating the magnitude of thalamic feedback onto the apical dendrites. In particular we were able to reproduce both the stepwise increase in the speed of perceptual reversals that accompanies parametric manipulations of attention, and the stepwise equivalency between attention and stimulus strength. Finally, we showed that the biasing effect of expectation on the initial competition for perceptual dominance was well described by the introduction of an additional source of apical drive, reproducing the empirically observed effect of both valid and invalid expectation on breakthrough time in continuous flash suppression (Pinto et al., 2015). A notable difference between our spiking model and canonical algorithmic models of top-down prediction which incorporate an explicit role for expectation such as predictive coding is that in our model, in line with empirical recordings from LV_{PT} cells, feedback has an amplifying effect on neural activity similar to adaptive resonance theory (Grossberg, 1995; Raizada & Grossberg, 2003), whereas, in most predictive coding models (Bastos et al., 2012; Friston, 2018; Rao & Ballard, 1999) feedback suppresses activity. We note, however, that this is not true of all predictive coding models, some implementations cast feedback as excitatory (Spratling, 2017). In addition, the implementation of predictive coding in spiking neurons is an open question and the effect of feedback is likely to be layer-specific. For example, Mikulasch et al, (2023) propose that in layer II/III feedback has a net suppressive effect on pyramidal cell activity whereas activity in LV_{PT} cells is enhanced by feedback.

By building a model based on circuitry identified in a rodent model of conscious perception that is able to reproduce the behaviour of human participants, we hope to help bridge the gap between the cognitive and cellular level study of consciousness. With this aim in mind, we conclude by highlighting three additional predictions that bridge microscopic and macroscopic scales. One, perceptual dominance should be characterised by bursting in LV_{PT} cells, a prediction that with recent advances in recording technology (Trautmann et al., 2023) and experimental techniques (Bogatova et al., 2022; Palagina et al., 2017) can currently be tested in mouse models and may soon be testable in non-human primates. Two, changes in perceptual dominance in visual rivalry should be evident in matrix nuclei of the thalamus (which forms a closed loop with LV_{PT} cells; Mease & Gonzalez, 2021). This prediction has, in fact, already received partial support from a recent fMRI study investigating the neural correlates of perception in a bistable colour illusion paradigm which found that matrix nuclei but not core nuclei distinguished between fused and non-fused perception (Seo et al., 2022). Three, by hypothesis, expectation, like attention, modulates the gain of LV_{PT} cells, therefore the biasing effect of predictive cues on the initial competition for dominance in binocular rivalry should be equivalent to a stepwise increase in stimulus strength to the same eye and be compensated for by a stepwise decrease in stimulus strength to the same eye.

Online Methods

The neuronal backbone of the model consists of 'Izhikevich' quadratic adaptive integrate and fire neurons, a variety of hybrid dynamical system that, with biophysically fit parameters, is capable of reproducing a wide variety of the spiking behaviour whilst still being highly efficient to integrate numerically (Izhikevich, 2003, 2004, 2006).

$$C\dot{v} = k(v(t) - v_r)(v(t) - v_t) - u(t) + I_{ext} \tag{1}$$

$$\dot{u} = a\{b(v(t) - v_r) - u(t)\} \tag{2}$$

With the following reset conditions: if $v \geq v_{peak}$ then $v \rightarrow c, u \rightarrow u + d$. The equations are in dimensional form giving the membrane potential (including the resting potential v_r, spike threshold v_t, and spike peak v_{peak}), input I_{ext}, time t, and capacitance C, biophysically

interpretable units (microvolts, picoamperes, milliseconds, and picofarads respectively).The remaining three parameters k, a, and b, are dimensionless and control the timescale of the membrane potential, the timescale of spike adaptation, and the sensitivity of spike adaptation to sub-threshold oscillations. Crucially, Izhikevich (Izhikevich, 2006; Izhikevich & Edelman, 2008) fit parameters for a large class of cortical and sub-cortical neurons, thus affording our model a high degree of neurobiological plausibility while greatly reducing the number of free parameters.

The model included three classes of neurons: LV_{PT} cells, fast spiking interneurons (basket cells), and matrix thalamic cells (**Fig 1 A-C**). The parameters for the fast spiking interneurons and thalamic cells were taken unmodified from Izhikevich and Edelman (2008). For the LV_{PT} cells we employed a novel dual compartment neuron with (coupled) apical and basal compartments, each described by equations (1) to (2), allowing us to reproduce the change in dynamical regime in LV_{PT} cells that occurs when they receive coincident apical and basal drive. We leveraged the insight (Izhikevich, 2003; Munn et al., 2023) that the difference between regular spiking and bursting behaviour can be modelled by changing the reset conditions of equations (1) and (2) - raising the reset voltage (increasing c) taking the neuron closer to threshold, and reducing the magnitude of spike adaptation (decreasing d). We set up the coupling between compartments such that the apical compartment controlled the reset conditions on the somatic compartment with an apical spike switching the reset conditions of the somatic compartment from regular spiking to bursting parameters for 25 ms. In turn, the membrane potential of the apical compartment was coupled to the somatic compartment by adding a conductance term ($20(v_{soma} - v_{dendrite})$) to equation (1) allowing for somatic spikes to back propagate and contribute to the generation of spikes in the apical compartment. Parameters of equations (1) – (2) for each neuron/compartment are given in **table 1**.

Neuron	C	k	v_r	v_t	a	b	c	d	v_{peak}
LV_{PT} dendrite	100 pF	1	− 50 mV	− 50 mV	0.8	15	−10	500	20 mV
LV_{PT} soma	150 pF	1.2	− 75 mV	− 45 mV	0.01	5	Reg: − 66 Burst: − 56	Reg: 260 Burst: 130	50 mV
Basket cell	20 pF	1	− 55 mV	− 40 mV	0.15	8	− 55	200	25 mV
Matrix thalamus	200 pF	1.6	− 60 mV	− 50 mV	0.01	15	− 60	10	35 mV

Table 1. Parameters for each class of Izhikevich neuron. LV_{PT} dendrite and soma parameters were modified from the active dendrite multi-compartment model (p.293) and intrinsic bursting model (p.290) described in Izhikevich (2006). Basket cell (fast spiking interneuron), and matrix thalamus parameters were taken, unmodified, from Izhikevich and Edelman (2008).

Based on previous spiking neural network models of rivalry (Laing et al., 2010; Laing & Chow, 2002; Wang et al., 2020) the cortical component of the network had a one-dimensional ring architecture. Each point on the ring represents an orientation preference with one full rotation around the ring corresponding to a 180° visual rotation. This mirrors the fact that a 180° rotation of a grating results in a visually identical stimulus and also ensures periodic boundary conditions. The cortical ring contained 90 LV_{PT} neurons and 90 fast spiking interneurons. Each pair of excitatory and inhibitory neurons was assigned to an equidistant location on the ring (unit circle) giving each neuron a 2° difference in orientation preference relative to each of its neighbours. The (dimensionless) synaptic weights $w_{i,j}^{\kappa\omega}$ connecting neurons ($E \rightarrow E$, $I \rightarrow E$, and $E \rightarrow I$), were all to all with magnitudes decaying as a function of the Euclidean distance $\delta_{i,j}$ between neurons (equations (3)) according to a spatial Gaussian footprint (equation (4)).

$$\delta_{i,j} = \sqrt{(\cos\theta_i - \cos\theta_j)^2 + (\sin\theta_i - \sin\theta_j)^2} \tag{3}$$

$$w_{i,j}^{\kappa\omega} = \lambda^{\kappa\omega} e^{-\frac{1}{2}\left(\frac{\delta_{i,j}}{\sigma^{\kappa\omega}}\right)^2} \tag{4}$$

Where θ is the location of the neuron on the unit circle, κ and ω denote the pre- and post-synaptic neuron, λ controls the magnitude of the synaptic weights, and $\sigma^{\kappa\omega}$ the spatial spread. In line with empirical constraints inhibitory coupling had a larger spatial spread and magnitude than excitatory to excitatory coupling (Naka & Adesnik, 2016). Each 9 cortical neurons were coupled to 1 thalamic neuron which then projected back up to the apical dendrites of the same 9 cortical neurons in line with the diffuse projections of higher order thalamus onto the apical dendrites of LV_{PT} neurons in layer I (Mease & Gonzalez, 2021; Shepherd & Yamawaki, 2021). For simplicity we set projections to from the thalamus to a constant value (e.g., $w_{i,j}^{TH\rightarrow D} = \lambda^{TH\rightarrow D}$). Synapses had a bi-exponential form (equation (5)) with rise (τ_{rise}) and decay (τ_{decay}) constants chosen to recapitulate the dynamics of inhibitory ($GABA_A$), and excitatory (AMPA and NMDA) synapses (Dayan & Abbott, 2005; Gerstner et al., 2014).

$$g_i(t)_{syn} = \sum_j w_{i,j}^{\kappa\omega} g_\infty \left(1 - e^{-\frac{(t-t_j^f)}{\tau_{rise}}}\right) e^{-\frac{(t-t_j^f)}{\tau_{decay}}} \Theta(t - t_j^f) \tag{5}$$

We set g_∞ to 1 for GABA$_A$ and AMPA synapses, and $g_\infty = \frac{1}{1+[Mg^{2+}]\beta e^{-\alpha v_i(t)}}$ for NMDA synapses making the conductance voltage sensitive, where Θ denotes the Heaviside function, and t^f is the time that the neuron passes the threshold $v \geq v_{peak}$. The conductance term entered into the input I_{ext} through the relation $I_{i,syn} = g_i(t)_{syn}(E_{syn} - v_i(t))$ where E_{syn} is the reverse potential of the synapse.

External drive into the model exclusively targeted the somatic compartment of LV$_{PT}$ cells representing input into the basal dendrites. We decomposed the external drive into four terms, $I_{ext} = I_C + I_{AMPA} + I_{NMDA} + I_{adapt}$, consisting of a (subthreshold) constant drive (I_C), two glutamatergic conductance based terms ($I_{AMPA} + I_{NMDA}$), and a slow hyperpolarising adaptation current I_{adapt}. We obtained I_{AMPA} and I_{NMDA} by convolving a stochastic Poisson spike train with equation (5). Separate monocular inputs into the network were modelled with independent Poisson processes (representing input from the left and right eyes with rates varying between 450 Hz and 525 Hz depending on the simulation). The constant drive took the neuron closer to threshold reducing the firing rate of the conductance based input necessary to drive the model circumventing a number of known numerical issues that arise when conductance values get too large (Izhikevich, 2010). The adaptation current was described by $I_{adapt} = g_i(t)_{adapt}(E_{adapt} - v_i(t))$ with $g_i(t)_{adapt}$ obtained from numerical integration of equation (6).

$$\dot{g}_{adapt} = -\frac{g(t)_{adapt}}{\tau_{adapt}} + \Delta g \delta(t - t^{tf}) \tag{6}$$

Where Δg is the contribution of each spike to the hyperpolarising current and τ_{adapt} the time constant. External drive (with the exception of I_{adapt}) was weighted by the spatial Gaussian shown in equation (7) centred on neurons 90° apart on the ring (i.e., 45 neurons apart) corresponding to the orthogonal grating stimuli commonly employed in binocular rivalry experiments.

$$h_i = e^{-\left(\frac{(i-N_L)}{\sigma^{\varepsilon}}\right)^2} + e^{-\left(\frac{(i-N_R)}{\sigma^{\varepsilon}}\right)^2} \tag{7}$$

Here i denotes the index of the ith neuron, N_L and N_R control the orientation of the stimulus delivered to the left and right eyes, and σ^{ε} controls the spatial spread with the superscript indicating the source of the external drive (i.e., feedforward stimulus drive vs feedback projections). To model continuous flash suppression we increased the external drive centred on N_L from 300 Hz to 500 Hz and decreased the external drive entering centred on N_R from 300 Hz to 500 Hz in steps of ~ 3 Hz every 100 ms over a 6 second simulation period.

The equations were integrated numerically in MATLAB using the hybrid scheme introduced by Izhikevich (2010) with a step size of 1 ms, along with a linear interpolation method, that adjusts the integration step size of spike adaptation in line with the timing of the spike (i.e. inferring the value t when $v(t) = v_{peak}$ rather than just taking the value of t when $v(t) \geq v_{peak}$).

Simulations of Levelt's propositions were run for 120 s, all subsequent simulations, which swept over a larger number of parameter, were run for 60 s. To ensure robustness all results shown in the main text were averaged over 40 random seeds. We defined perceptual dominance in terms of the average firing rate of neurons on opposite sides of the ring which we treated as separate populations. Due to the fluctuations in the average firing rate of each population we required that a population have a 5 Hz greater firing rate than the other to be counted as dominant. Parameters for the model components described by equations (3) – (7) are supplied in **table 2**.

Parameter	Description	Value
$\lambda^{E\to E}$	Magnitude of excitatory to excitatory coupling	$\frac{3.25}{\sigma^{E\to E}\sqrt{2\pi}}$
$\lambda^{E\to I}$	Magnitude of excitatory to inhibitory coupling	$\frac{1}{\sigma^{E\to I}\sqrt{2\pi}}$
$\lambda^{I\to E}$	Magnitude of inhibitory to excitatory coupling	$\frac{4.5}{\sigma^{I\to E}\sqrt{2\pi}}$
$\lambda^{E\to TH}$	Constant excitatory to thalamic coupling constant	4
$\lambda^{TH\to D}$	Constant thalamic to apical dendrite coupling	1
$\sigma^{E\to E}$	Spread of excitatory to excitatory coupling	0.5
$\sigma^{E\to I}$	Spread of excitatory to inhibitory coupling	2
$\sigma^{I\to E}$	Spread of inhibitory to excitatory coupling	2
τ_{rise}: AMPA	Rise time of AMPA conductance	1 ms

τ_{decay}: AMPA	Decay time of AMPA conductance	8 ms
τ_{rise}: $GABA_A$	Rise time of $GABA_A$ conductance	1 ms
τ_{decay}: $GABA_A$	Decay time of $GABA_A$ conductance	6 ms
τ_{rise}: NMDA	Rise time of NMDA conductance	10 ms
τ_{decay}: NMDA	Decay time of NMDA conductance	75 ms
Mg^{2+}	Extracellular magnesium concentration	1.2 mM
β	Backward rate constant of voltage dependent NMDA conductance	3.57^{-1} mM
α	Forward rate constant of voltage dependent NMDA conductance	0.062 mV
τ_{adapt}	Decay time of adaptation current	2000 ms
Δg	Contribution of each spike to adaptation current	0.045 nS
σ^{ext}	Spatial spread of external drive	10
σ^{dend}	Spatial spread of apical drive	5
I_C	Constant component of external drive	200 pS

Table 2. Parameter description and values for the components of the model described by equations (3) – (7)

Supplementary Material

Dynamical Regime

To interrogate the structure of the dynamical system underlying the stochastic oscillations we ran the model with constant drive and asymmetric initial conditions that ensured that the system converged to a state where one of the populations was dominant whilst the other was suppressed. We reasoned that if the oscillations were driven by stochastic jumps between stable fixed points with basins of attraction only weakly affected by adaptation then in the absence of noise oscillations should disappear. In contrast, if adaptation exerts a large effect, the stochastic oscillations should consist of noisy excursions around a stable limit cycle and the model should continue to oscillate in the absence of noise (c.f. Moreno-Bote et al., 2007; Shpiro et al., 2009). In agreement with the stable limit cycle hypothesis in the absence of noise the model continued to oscillate (**Fig S1A**). To test the stability of the limit cycle we: i) confirmed the existence of an unstable structure inside the limit cycle; and ii) confirmed that perturbations to the limit cycle decayed back to a stable orbit. Indeed, with symmetric initial conditions the model converged to a state where excitatory activity on each side of the ring was perfectly matched. Perturbations to this state consisting of a 1 ms pulse of constant drive (50 pS) delivered to the basal dendrites of the somatic compartment of a single LV_{PT} neuron caused the orbit to

converge to the surrounding limit cycle (**Fig S1B**). Such perturbations had little effect on already oscillating orbits confirming the stability of the limit cycle (**Fig S1B**).

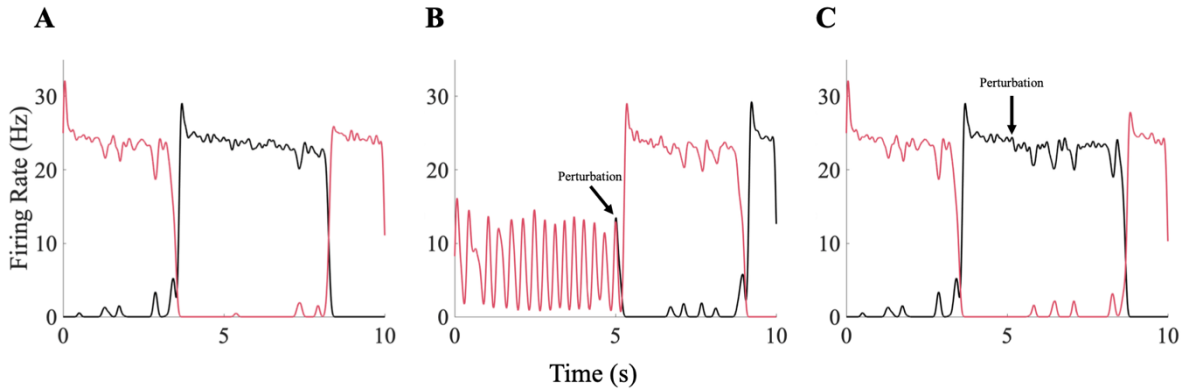

Figure S1. A) Average firing rate of neuronal populations on opposite ends of the ring driven by constant drive with asymmetric initial conditions that ensured the population represented by the pink line would win the initial competition for dominance. **B)** Average firing rate of neuronal populations simulated with constant drive and symmetric initial conditions. A perturbation was delivered at $t = 5000$ sending the population orbit to the surrounding stable limit cycle. **C)** Average firing rate of neuronal populations driven by constant drive with asymmetric initial conditions. Perturbation delivered at $t = 5000$ had no substantial effect on the already oscillating orbit indicative of a stable limit cycle.

Code and Data Availability

MATLAB code illustrating the basic operation of the model can be found at https://github.com/cjwhyte/LV_VisualRivalry. Complete code, and simulated data, will be made available upon full publication of the paper.

Acknowledgements

We are grateful to Michael Breakspear and Bryan Paton for discussion on an early iteration of the model described in this paper.

References

Alais, D., & Blake, R. (2005). *Binocular Rivalry*. MIT Press.

Aru, J., Siclari, F., Phillips, W. A., & Storm, J. F. (2020). Apical drive—A cellular mechanism of dreaming? *Neuroscience & Biobehavioral Reviews*, *119*, 440–455. https://doi.org/10.1016/j.neubiorev.2020.09.018

Aru, J., Suzuki, M., & Larkum, M. E. (2020). Cellular Mechanisms of Conscious Processing. *Trends in Cognitive Sciences*, *24*(10), 814–825. https://doi.org/10.1016/j.tics.2020.07.006

Aru, J., Suzuki, M., Rutiku, R., Larkum, M. E., & Bachmann, T. (2019). Coupling the State and Contents of Consciousness. *Frontiers in Systems Neuroscience*, *13*, 43. https://doi.org/10.3389/fnsys.2019.00043

Bastos, A. M., Lundqvist, M., Waite, A. S., Kopell, N., & Miller, E. K. (2020). *Layer and rhythm specificity for predictive routing* [Preprint]. Neuroscience. https://doi.org/10.1101/2020.01.27.921783

Bastos, A. M., Usrey, W. M., Adams, R. A., Mangun, G. R., Fries, P., & Friston, K. J. (2012). Canonical Microcircuits for Predictive Coding. *Neuron*, *76*(4), 695–711. https://doi.org/10.1016/j.neuron.2012.10.038

Bastos, A. M., Vezoli, J., Bosman, C. A., Schoffelen, J.-M., Oostenveld, R., Dowdall, J. R., De Weerd, P., Kennedy, H., & Fries, P. (2015). Visual Areas Exert Feedforward and Feedback Influences through Distinct Frequency Channels. *Neuron*, *85*(2), 390–401. https://doi.org/10.1016/j.neuron.2014.12.018

Blake, R., & Tong, F. (2008). Binocular rivalry. *Scholarpedia*, *3*(12), 1578. https://doi.org/10.4249/scholarpedia.1578

Bogatova, D., Smirnakis, S. M., & Palagina, G. (2022). *Tug-of-peace: Visual Rivalry and Atypical Visual Motion Processing in MECP2 duplication Syndrome of Autism* [Preprint]. Neuroscience. https://doi.org/10.1101/2022.09.23.509144

Bonneh, Y. S., Donner, T. H., Cooperman, A., Heeger, D. J., & Sagi, D. (2014). Motion-Induced Blindness and Troxler Fading: Common and Different Mechanisms. *PLoS ONE*, *9*(3), e92894. https://doi.org/10.1371/journal.pone.0092894

Brascamp, J. W., Klink, P. C., & Levelt, W. J. M. (2015). The 'laws' of binocular rivalry: 50 years of Levelt's propositions. *Vision Research*, *109*, 20–37. https://doi.org/10.1016/j.visres.2015.02.019

Brascamp, J. W., van Ee, R., Noest, A. J., Jacobs, R. H. A. H., & van den Berg, A. V. (2006). The time course of binocular rivalry reveals a fundamental role of noise. *Journal of Vision*, *6*(11), 8–8. https://doi.org/10.1167/6.11.8

Brown, R., Lau, H., & LeDoux, J. (2019). *The Misunderstood Higher-Order Approach to Consciousness* [Preprint]. PsyArXiv. https://doi.org/10.31234/osf.io/xpy8h

Buckthought, A., Kim, J., & Wilson, H. R. (2008). Hysteresis effects in stereopsis and binocular rivalry. *Vision Research*, *48*(6), 819–830. https://doi.org/10.1016/j.visres.2007.12.013

Carmel, D., Arcaro, M., Kastner, S., & Hasson, U. (2010). How to Create and Use Binocular Rivalry. *Journal of Visualized Experiments*, *45*, 2030. https://doi.org/10.3791/2030

Chao, H.-T., Chen, H., Samaco, R. C., Xue, M., Chahrour, M., Yoo, J., Neul, J. L., Gong, S., Lu, H.-C., Heintz, N., Ekker, M., Rubenstein, J. L. R., Noebels, J. L., Rosenmund, C., & Zoghbi, H. Y. (2010). Dysfunction in GABA signalling mediates autism-like stereotypies and Rett syndrome phenotypes. *Nature*, *468*(7321), Article 7321. https://doi.org/10.1038/nature09582

Crick, F., & Koch, C. (2003). A framework for consciousness. *Nature Neuroscience*, *6*(2), Article 2. https://doi.org/10.1038/nn0203-119

Dayan, P., & Abbott, L. F. (2005). *Theoretical Neuroscience: Computational and Mathematical Modeling of Neural Systems*. MIT Press.

Denison, R. N., Piazza, E. A., & Silver, M. A. (2011). Predictive Context Influences Perceptual Selection during Binocular Rivalry. *Frontiers in Human Neuroscience*, *5*. https://doi.org/10.3389/fnhum.2011.00166

Friston, K. (2005). A theory of cortical responses. *Philosophical Transactions of the Royal Society B: Biological Sciences*, *360*(1456), 815–836. https://doi.org/10.1098/rstb.2005.1622

Friston, K. (2018). Does predictive coding have a future? *Nature Neuroscience*, *21*(8), 1019–1021. https://doi.org/10.1038/s41593-018-0200-7

Gerstner, W., Kistler, W. M., Naud, R., & Paninski, L. (2014). *Neuronal Dynamics: From Single Neurons to Networks and Models of Cognition* (1st ed.). Cambridge University Press. https://doi.org/10.1017/CBO9781107447615

Giles, N., Lau, H., & Odegaard, B. (2016). What Type of Awareness Does Binocular Rivalry Assess? *Trends in Cognitive Sciences*, *20*(10), 719–720. https://doi.org/10.1016/j.tics.2016.08.010

Grossberg, S. (1995). The Attentive Brain. *American Scientist*, *83*(5), 438–449.

Grossberg, S., Yazdanbakhsh, A., Cao, Y., & Swaminathan, G. (2008). How does binocular rivalry emerge from cortical mechanisms of 3-D vision? *Vision Research*, *48*(21), 2232–2250. https://doi.org/10.1016/j.visres.2008.06.024

Guo, K., Yamawaki, N., Barrett, J. M., Tapies, M., & Shepherd, G. M. G. (2020). Cortico-Thalamo-Cortical Circuits of Mouse Forelimb S1 Are Organized Primarily as

Recurrent Loops. *The Journal of Neuroscience*, *40*(14), 2849–2858. https://doi.org/10.1523/JNEUROSCI.2277-19.2020

Halassa, M. M., & Kastner, S. (2017). Thalamic functions in distributed cognitive control. *Nature Neuroscience*, *20*(12), Article 12. https://doi.org/10.1038/s41593-017-0020-1

Harris, K. D., & Shepherd, G. M. G. (2015). The neocortical circuit: Themes and variations. *Nature Neuroscience*, *18*(2), 170–181. https://doi.org/10.1038/nn.3917

Izhikevich, E. M. (2003). Simple model of spiking neurons. *IEEE Transactions on Neural Networks*, *14*(6), 1569–1572. https://doi.org/10.1109/TNN.2003.820440

Izhikevich, E. M. (2004). Which model to use for cortical spiking neurons? *IEEE Transactions on Neural Networks*, *15*(5), 1063–1070. https://doi.org/10.1109/TNN.2004.832719

Izhikevich, E. M. (2006). *Dynamical Systems in Neuroscience: The Geometry of Excitability and Bursting*. The MIT Press. https://doi.org/10.7551/mitpress/2526.001.0001

Izhikevich, E. M. (2010). Hybrid spiking models. *Philosophical Transactions of the Royal Society A: Mathematical, Physical and Engineering Sciences*, *368*(1930), 5061–5070. https://doi.org/10.1098/rsta.2010.0130

Izhikevich, E. M., & Edelman, G. M. (2008). Large-scale model of mammalian thalamocortical systems. *Proceedings of the National Academy of Sciences*, *105*(9), 3593–3598. https://doi.org/10.1073/pnas.0712231105

John, Y. J., Zikopoulos, B., Bullock, D., & Barbas, H. (2018). *Visual Attention Decits in Schizophrenia Can Arise From Inhibitory Dysfunction in Thalamus or Cortex* (0). *2*(0), Article 0. https://doi.org/10.1162/CPSY_a_00023

Kastner, S., Fiebelkorn, I. C., & Eradath, M. K. (2020). Dynamic pulvino-cortical interactions in the primate attention network. *Current Opinion in Neurobiology*, *65*, 10–19. https://doi.org/10.1016/j.conb.2020.08.002

Laing, C. R., & Chow, C. C. (2002). A Spiking Neuron Model for Binocular Rivalry. *Journal of Computational Neuroscience*, *12*(1), 39–53. https://doi.org/10.1023/A:1014942129705

Laing, C. R., Frewen, T., & Kevrekidis, I. G. (2010). Reduced models for binocular rivalry. *Journal of Computational Neuroscience*, *28*(3), 459–476. https://doi.org/10.1007/s10827-010-0227-6

Lamme, V. A. F. (2006). Towards a true neural stance on consciousness. *Trends in Cognitive Sciences*, *10*(11), 494–501. https://doi.org/10.1016/j.tics.2006.09.001

Larkum, M. E. (2004). Top-down Dendritic Input Increases the Gain of Layer 5 Pyramidal Neurons. *Cerebral Cortex*, *14*(10), 1059–1070. https://doi.org/10.1093/cercor/bhh065

Larkum, M. E. (2022). Are Dendrites Conceptually Useful? *Neuroscience*, *489*, 4–14. https://doi.org/10.1016/j.neuroscience.2022.03.008

Larkum, M. E., Nevian, T., Sandler, M., Polsky, A., & Schiller, J. (2009). Synaptic Integration in Tuft Dendrites of Layer 5 Pyramidal Neurons: A New Unifying Principle. *Science*, *325*(5941), 756–760. https://doi.org/10.1126/science.1171958

Leopold, D. A., & Logothetis, N. K. (1996). Activity changes in early visual cortex reflect monkeys' percepts during binocular rivalry. *Nature*, *379*(6565), 549–553. https://doi.org/10.1038/379549a0

Levelt, W. J. M. (1965). *On Binocular Rivalry* [Institute for Perception]. https://www.mpi.nl/world/materials/publications/levelt/Levelt_Binocular_Rivalry_1965.pdf

Levelt, W. J. M. (1967). Note on the Distribution of Dominance Times in Binocular Rivalry. *British Journal of Psychology*, *58*(1–2), 143–145. https://doi.org/10.1111/j.2044-8295.1967.tb01068.x

Logothetis, N. K., & Leopold, D. A. (1996). *What is rivalling during binocular rivalry? 380*.

Mashour, G. A., Roelfsema, P., Changeux, J.-P., & Dehaene, S. (2020). Conscious Processing and the Global Neuronal Workspace Hypothesis. *Neuron*, *105*(5), 776–798. https://doi.org/10.1016/j.neuron.2020.01.026

Mease, R. A., & Gonzalez, A. J. (2021). Corticothalamic Pathways From Layer 5: Emerging Roles in Computation and Pathology. *Frontiers in Neural Circuits*, *15*, 730211. https://doi.org/10.3389/fncir.2021.730211

Meng, M., & Tong, F. (2004). Can attention selectively bias bistable perception? Differences between binocular rivalry and ambiguous figures. *Journal of Vision*, *4*(7), 2. https://doi.org/10.1167/4.7.2

Mikulasch, F. A., Rudelt, L., Wibral, M., & Priesemann, V. (2023). Where is the error? Hierarchical predictive coding through dendritic error computation. *Trends in Neurosciences*, *46*(1), 45–59. https://doi.org/10.1016/j.tins.2022.09.007

Moreno-Bote, R., Rinzel, J., & Rubin, N. (2007). Noise-Induced Alternations in an Attractor Network Model of Perceptual Bistability. *Journal of Neurophysiology*, *98*(3), 1125–1139. https://doi.org/10.1152/jn.00116.2007

Munn, B. R., Müller, E. J., & Shine, J. M. (2023). *Noradrenergic neuromodulation of nonlinear bursting neurons controls critical dynamics* (arXiv:2106.07865). arXiv. http://arxiv.org/abs/2106.07865

Naka, A., & Adesnik, H. (2016). Inhibitory Circuits in Cortical Layer 5. *Frontiers in Neural Circuits*, *10*. https://doi.org/10.3389/fncir.2016.00035

Overgaard, M. (2015). *Behavioural Methods in Consciousness Research*. Oxford University Press.

Paffen, C., & Alais, D. (2011). Attentional Modulation of Binocular Rivalry. *Frontiers in Human Neuroscience*, *5*. https://www.frontiersin.org/articles/10.3389/fnhum.2011.00105

Paffen, C. L. E., Alais, D., & Verstraten, F. A. J. (2006). Attention Speeds Binocular Rivalry. *Psychological Science*, *17*(9), 752–756. https://doi.org/10.1111/j.1467-9280.2006.01777.x

Palagina, G., Meyer, J. F., & Smirnakis, S. M. (2017). Complex Visual Motion Representation in Mouse Area V1. *The Journal of Neuroscience*, *37*(1), 164–183. https://doi.org/10.1523/JNEUROSCI.0997-16.2017

Pinto, Y., van Gaal, S., de Lange, F. P., Lamme, V. A. F., & Seth, A. K. (2015). Expectations accelerate entry of visual stimuli into awareness. *Journal of Vision*, *15*(8), 13. https://doi.org/10.1167/15.8.13

Raizada, R. D. S., & Grossberg, S. (2003). Towards a Theory of the Laminar Architecture of Cerebral Cortex: Computational Clues from the Visual System. *Cerebral Cortex*, *13*(1), 100–113. https://doi.org/10.1093/cercor/13.1.100

Rao, R. P. N., & Ballard, D. H. (1999). Predictive coding in the visual cortex: A functional interpretation of some extra-classical receptive-field effects. *Nature Neuroscience*, *2*(1), 79–87. https://doi.org/10.1038/4580

Safavi, S., & Dayan, P. (2022). Multistability, perceptual value, and internal foraging. *Neuron*, S0896627322006699. https://doi.org/10.1016/j.neuron.2022.07.024

Schmitt, L. I., Wimmer, R. D., Nakajima, M., Happ, M., Mofakham, S., & Halassa, M. M. (2017). Thalamic amplification of cortical connectivity sustains attentional control. *Nature*, *545*(7653), Article 7653. https://doi.org/10.1038/nature22073

Seo, J., Kim, D.-J., Choi, S.-H., Kim, H., & Min, B.-K. (2022). The thalamocortical inhibitory network controls human conscious perception. *NeuroImage*, *264*, 119748. https://doi.org/10.1016/j.neuroimage.2022.119748

Seth, A. K., & Bayne, T. (2022). Theories of consciousness. *Nature Reviews Neuroscience*, *23*(7), 439–452. https://doi.org/10.1038/s41583-022-00587-4

Shai, A. S., Anastassiou, C. A., Larkum, M. E., & Koch, C. (2015). Physiology of Layer 5 Pyramidal Neurons in Mouse Primary Visual Cortex: Coincidence Detection through Bursting. *PLOS Computational Biology*, *11*(3), e1004090. https://doi.org/10.1371/journal.pcbi.1004090

Shepherd, G. M. G., & Yamawaki, N. (2021). Untangling the cortico-thalamo-cortical loop: Cellular pieces of a knotty circuit puzzle. *Nature Reviews Neuroscience*, *22*(7), 389–406. https://doi.org/10.1038/s41583-021-00459-3

Shine, J. M., Lewis, L. D., Garrett, D. D., & Hwang, K. (2023). The impact of the human thalamus on brain-wide information processing. *Nature Reviews Neuroscience*. https://doi.org/10.1038/s41583-023-00701-0

Shpiro, A., Curtu, R., Rinzel, J., & Rubin, N. (2007). Dynamical Characteristics Common to Neuronal Competition Models. *Journal of Neurophysiology*, *97*(1), 462–473. https://doi.org/10.1152/jn.00604.2006

Shpiro, A., Moreno-Bote, R., Rubin, N., & Rinzel, J. (2009). Balance between noise and adaptation in competition models of perceptual bistability. *Journal of Computational Neuroscience*, *27*(1), 37–54. https://doi.org/10.1007/s10827-008-0125-3

Spratling, M. W. (2017). A review of predictive coding algorithms. *Brain and Cognition*, *112*, 92–97. https://doi.org/10.1016/j.bandc.2015.11.003

Takahashi, N., Ebner, C., Sigl-Glöckner, J., Moberg, S., Nierwetberg, S., & Larkum, M. E. (2020). Active dendritic currents gate descending cortical outputs in perception. *Nature Neuroscience*, *23*(10), 1277–1285. https://doi.org/10.1038/s41593-020-0677-8

Takahashi, N., Oertner, T. G., Hegemann, P., & Larkum, M. E. (2016). Active cortical dendrites modulate perception. *Science*, *354*(6319), 1587–1590. https://doi.org/10.1126/science.aah6066

Tong, F., Meng, M., & Blake, R. (2006). Neural bases of binocular rivalry. *Trends in Cognitive Sciences*, *10*(11), 502–511. https://doi.org/10.1016/j.tics.2006.09.003

Tononi, G., Boly, M., Massimini, M., & Koch, C. (2016). Integrated information theory: From consciousness to its physical substrate. *Nature Reviews Neuroscience*, *17*(7), 450–461. https://doi.org/10.1038/nrn.2016.44

Trautmann, E. M., Hesse, J. K., Stine, G. M., Xia, R., Zhu, S., O'Shea, D. J., Karsh, B., Colonell, J., Lanfranchi, F. F., Vyas, S., Zimnik, A., Steinmann, N. A., Wagenaar, D. A., Andrei, A., Lopez, C. M., O'Callaghan, J., Putzeys, J., Raducanu, B. C., Welkenhuysen, M., … Harris, T. (2023). *Large-scale high-density brain-wide neural recording in nonhuman primates* [Preprint]. Neuroscience. https://doi.org/10.1101/2023.02.01.526664

Valuch, C., & Kulke, L. (2020). Predictive context biases binocular rivalry in children and adults with no positive relation to two measures of social cognition. *Scientific Reports*, *10*(1), 2059. https://doi.org/10.1038/s41598-020-58921-8

Wang, Z., Dai, W., & McLaughlin, D. W. (2020). Ring models of binocular rivalry and fusion. *Journal of Computational Neuroscience*, *48*(2), 193–211. https://doi.org/10.1007/s10827-020-00744-7

Wilson, H. R. (2003). Computational evidence for a rivalry hierarchy in vision. *Proceedings of the National Academy of Sciences*, *100*(24), 14499–14503. https://doi.org/10.1073/pnas.2333622100

Wilson, H. R. (2007). Minimal physiological conditions for binocular rivalry and rivalry memory. *Vision Research*, *47*(21), 2741–2750. https://doi.org/10.1016/j.visres.2007.07.007

Wilson, H. R. (2017). Binocular contrast, stereopsis, and rivalry: Toward a dynamical synthesis. *Vision Research*, *140*, 89–95. https://doi.org/10.1016/j.visres.2017.07.016

Wimmer, V. C., Bruno, R. M., De Kock, C. P. J., Kuner, T., & Sakmann, B. (2010). Dimensions of a Projection Column and Architecture of VPM and POm Axons in Rat Vibrissal Cortex. *Cerebral Cortex*, *20*(10), 2265–2276. https://doi.org/10.1093/cercor/bhq068

Wolfe, J. M. (1983). Influence of Spatial Frequency, Luminance, and Duration on Binocular Rivalry and Abnormal Fusion of Briefly Presented Dichoptic Stimuli. *Perception*, *12*(4), 447–456. https://doi.org/10.1068/p120447

Zhou, H., Schafer, R. J., & Desimone, R. (2016). Pulvinar-Cortex Interactions in Vision and Attention. *Neuron*, *89*(1), 209–220. https://doi.org/10.1016/j.neuron.2015.11.034